Slow light and band gaps in metallodielectric cylinder arrays

Jeffrey M. Shainline and Jimmy Xu

Department of Physics and Division of Engineering, Brown University, 184 Hope St., Providence, RI, 02912

Jeffrey_Shainline@Brown.edu

http://opto.brown.edu

Abstract: We consider two-dimensional three-component photonic crystals wherein one component is modeled as a drude-dispersive metal. It is found that the dispersion relation of light in this environment depends critically on the configuration of the metallic and dielectric components. In particular, for the case of an incident electromagnetic wave with electric field vector parallel to the axis of the cylinders it is shown that the presence of dielectric shells covering the metallic cylinders leads to a closing of the structural band gap with increased filling factor, as would be expected for a purely dielectric photonic crystal. For the same polarization, the photonic band structure of an array of metallic shell cylinders with dielectric cores do not show the closing of the structural band gap with increased filling factor of the metallic component. In this geometry, the photonic band structure contains bands with very small values of group velocity with some bands having a maximum of group velocity as small as .05c.

© 2009 Optical Society of America

OCIS codes: (230.5298) Photonic crystals; (350.4238) Nanophotonics and photonic crystals; (160.3918) Metamaterials

---

References and links

1. E. Yablonovitch, "Inhibited Spontaneous Emission in Solid-State Physics and Electronics," Phys. Rev. Lett. **58,** 2059-2062 (1987).
2. S. John and R. Rangarajan, "Optimal structures for classical wave localization: an alternative to the ioffe-regel criterion," Phys. Rev. B **38,** 10101-10104 (1988).
3. R. Sprik, B.A. Van Tiggelen and A. Lagendijk, "Optical emission in periodic dielectrics," Europhys. Lett. **35,** 265-270 (1996).
4. T. Trifonov, L. F. Marsal, A. Rodriguez, J. Pallares and R. Alcubilla, "Analysis of photonic band gaps in two-dimensional photonic crystals with rods covered by a thin interfacial layer," Phys. Rev. B **70,** 195108-1-195108-8 (2004).
5. P. R. Evans, G. A. Wurtz, R. Atkinson, W. Hendren, D. O'Connor, W. Dickson, R. J. Pollard and A. V. Zayats, "Plasmonic core/shell nanorod arrays: subattoliter controlled geometry and tunable optical properties," J. Phys. Chem. C **111,** 12522-12527 (2007).
6. J. B. Pendry and A. MacKinnon, "Calculation of photon dispersion relations," Phys. Rev. Lett. **69,** 2772-2775 (1992).
7. K. Sakoda, N. Kawai, T. Ito, A. Chutinan, S. Noda, T. Mitsuyu and K. Hirao, "Photonic bands of metallic systems. I. Principle of calculation and accuracy," Phys. Rev. B **64,** 045116-1-045116-8 (2001).
8. T. Ito and K. Sakoda, "Photonic bands of metallic systems. II. Features of surface plasmon polaritons," Phys. Rev. B **64,** 045117-1-045117-8 (2001).
9. A. Christ, T. Zentgrafand, J. Kuhl, S. G. Tikhodeev, N. A. Gippius and H. Giessen, "Optical properties of planar metallic photonic crystal structures: Experiment and theory," Phys. Rev. B **70,** 125113-1-125113-15 (2004).

10. J. B. Pendry, "Photonic Band Structures," J. Mod. Opt. **41,** 209-229 (1994).
11. M. Plihal and A. A. Maradudin, "Photonic band structure of two-dimensional systems: The triangular lattice," Phys. Rev. B **44,** 8565-8571 (1991).
12. A. Glushko and L. Karachevtseva, "PBG properties of three-component 2D photonic crystals," Photonics and nanostructures-fundamentals and applications **4,** 141-145 (2006).
13. V. Kuzmiak and A.A. Maradudin, "Photonic band structures of one- and two-dimensional periodic systems with metallic components in the presence of dissipation," Phys. Rev. B **55,** 7427-7444 (1997).
14. V. Kuzmiak and A.A. Maradudin, "Distribution of electromagnetic field and group velocities in two-dimensional periodic systems with dissipative metallic components," Phys. Rev. B **58,** 7230-7251 (1998).
15. M. Kretschmann and A. A. Maradudin, "Band structures of two-dimensional surface-plasmon polaritonic crystals," Phys. Rev. B **66,** 245408-1-245408-8 (2002).
16. O. Sakai, T. Sakaguchi and K. Tachibana, "Photonic bands in two-dimensional microplasma arrays. I. Theoretical derivation of band structures of electromagnetic waves," J. Appl. Phys. **101,** 073304-1-07334-9 (2007).
17. T. Sakaguchi, O. Sakai and K. Tachibana, "Photonic bands and two-dimensional microplasma arrays. II. Band gaps observed in millimeter and subeterahertz ranges," J. Appl. Phys. **101,** 073305-1-07335-7 (2007).
18. C. Hafner, C. Xudong and R. Vahldieck, "Metallic photonic crystals at optical frequencies," Journal of computational and theoretical nanoscience **2,** 240-250 (2005).
19. R.-L. Chern, C. C. Chang and C. C. Chang, "Analysis of surface plasmon modes and band structures for plasmonic crystals in one and two dimensions," Phys. Rev. E **73,** 036605-1-036605-15 (2004).
20. C. C. H. Tang, "Backscattering from dielectric-coated infinite cylindrical obstacles," J. Appl. Phys. **28,** 628-633 (1957).
21. P. Nordlander and F. Le, "Plasmonic structure and electromagnetic field enhancements in the metallic nanoparticle-film system," Appl. Phys. B **84,** 35-41 (2006).

1. Introduction

Metamaterial environments have the potential to enhance or supress the emission of light as well as to slow light propagation and even achieve a negative index of refraction. Studies of periodic as well as aperiodic dielectric and metallic environments have been undertaken with the goal of devising systems which offer maximal control of the generation, storage and propagation of light. In particular, metamaterials composed of coupled metal and dielectric components with feature sizes comparable to or less than the wavelength of light display rich optical behavior such as negative index of refraction and slow pulse propagation. Systems with material periodicity on the scale of the wavelength of light have attracted much attention lately; the potential to engineer a modified vacuum in which the photonic density of states is modified to either enhance or suppress spontaneous emission has been of interest to many researchers[1, 2, 3, 4]. Additionally, creation of photonic environments wherein light traveling in all directions propagates significantly slower than in vacuum or with a negative index of refraction are important pursuits. Recent progress toward the fabrication of three component photonic crystals[5] demands theoretical consideration of the optical properties of such structures[4].

Methods of calculating photonic band structures have been developed over the last two decades. Amongst these are finite element methods [6], finite-difference time-domain (FDTD) [7, 8], scattering matrix [9], transfer matrix[10] and plane wave expansion methods [11, 12]. FDTD [7, 8], variations of the plane wave expansion technique [13, 14, 15, 16, 17], and other techniques [18, 19] have proven useful for calculating the photonic band structures of systems with metallic components arranged in a periodic array. However, most studies to date treat the metallic components with the free electron model, and damping is often neglected.

The present work is focused on two-dimensional periodic structures with one dielectric and one metallic component contained in a background dielectric, as depicted in Fig. 1. In particular, we extend the theoretical framework of the plane wave technique [11, 12, 13, 14] for the calculation of photonic band structures to three-component photonic crystals containing one metallic component. Dispersion and dissipation in the metallic regions of the photonic crystals are taken into consideration with a complex, frequency-dependent permittivity which we model
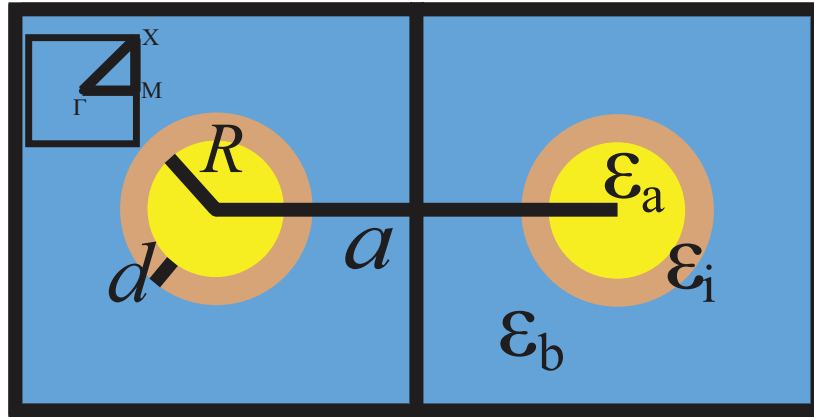
Fig. 1. The Wigner-Seitz cell of the two-dimensional three-component crystal. The lattice constant is a. The radius of the inner core cylinder is R. The thickness of the shell is d. The three dielectric regions are shown. The first Brillouin zone and points of high symmetry are shown in the inset.

as

$$\varepsilon(\omega) = 1 - \frac{\omega_p^2}{\omega(\omega + i\gamma)}. \tag{1}$$

We consider two dimensional arrays of infinite right circular cylinders arranged in a square lattice (see Fig. 1). The cylinders consist of either a metallic core surrounded by a dielectric shell or a dielectric core surrounded by a metallic shell. The cylinders are embedded in a homogeneous lossless medium, which without loss of generality is set to be vacuum in this work. The permittivity of the dielectric is treated as a constant. The main point of this study is to contrast the dispersion relation of the metallic core case with the metallic shell case. It is found that the metallic shell structures have far greater potential to reduce the group velocity of propagating modes, in some cases reducing it to .05 that in vacuum, nearly an order of magnitude less than the metallic core structures can achieve. The metallic shell structures also have far greater potential to give rise to structural band gaps.

For two-dimensional light propagation one can consider two orthogonal polarizations: the electric field perpendicular to the direction of propagation (parallel to the axis of the cylinders in our case, referred to as E-polarization), or the magnetic field perpendicular to the direction of propagation (H-polarization). The theoretical framework utilized in this report is based on a plane wave expansion. This approach converges nicely for E-polarization but encounters numerical convergence problems for H-polarization. For this reason, and because many of the unique physical features arise for E-polarized light in this geometry, we focus the rest of this paper on E-polarized electromagnetic fields.

The structure of this paper is as follows. In section 2 we discuss the theoretical methodology. In section 3 we analyze the photonic band structures of two-dimensional three component plasmonic crystals. The study is summarized in section 4. Aspects of the numerical treatment are discussed in the appendix.

2. Theoretical methodology

We consider electromagnetic waves propagating in the $x - y$ plane. We utilize the plane wave methodology [11, 13] wherein the dominant field component and the permittivity are expanded in the basis of plane waves. The following derivation results in a linear eigenvalue problem

which takes into consideration the Drude dispersion (including damping) of the metal. The derivation is similar to that presented in ref. [13], but is generalized in the present treatment to treat three-component photonic crystals with one metallic component. The z-component of the electric field and the material permittivity are expanded as

$$E_z(\mathbf{x}) = \sum_{\mathbf{G}} B(\mathbf{k}, \mathbf{G}) \exp(i(\mathbf{k} + \mathbf{G}) \cdot \mathbf{x}). \tag{2}$$

$$\varepsilon(\mathbf{x}, \omega) = \sum_{\mathbf{G}} \tilde{\varepsilon}(\mathbf{G}, \omega) \exp(i\mathbf{G} \cdot \mathbf{x}). \tag{3}$$

$\mathbf{x}$ is a vector in the $x - y$ plane and $\mathbf{G}$ is a vector of the reciprocal lattice. For the case of the square lattice $\mathbf{G} = (2\pi/a)(m\hat{x} + n\hat{y})$ where m and n are integers, $\hat{x}$ and $\hat{y}$ are unit vectors and a is the lattice constant, as shown in Fig. 1. The summations range over all m and n from negative to positive infinity; numerical investigations necessarily truncate the summation. The coefficients $\tilde{\varepsilon}$ are given by [12]

$$\tilde{\varepsilon}(\mathbf{G}, \omega) = \begin{cases} \varepsilon_b f_2 + \varepsilon_a f_1 + \varepsilon_i f_i, \\ \\ 2f_1(\varepsilon_a - \varepsilon_b)\frac{J_1(GR)}{GR} \\ +2f_i(\varepsilon_i - \varepsilon_b)\frac{J_1[G(R+d)]}{G(R+d)} \end{cases} \tag{4}$$

$\tilde{\varepsilon}$ depends on ω through the frequency dependence of either ε_a or ε_b. In Eqn. 4 the top element of the list is for $\mathbf{G} = 0$ and the bottom element for $\mathbf{G} \neq 0$. For a square lattice, $f_1 = \pi R^2/a^2$, $f_i = \pi(R+d)^2/a^2 - f_1$, $f_3 = \pi(R+d)^2/a^2$, and $f_2 = 1 - f_3$ [12]. From Maxwell's equations, one can derive the following partial differential equation obeyed by the dominant field component.

$$\left(\frac{\partial^2}{\partial x^2} + \frac{\partial}{\partial y^2} + \varepsilon(\mathbf{x}, \omega)\frac{\omega^2}{c^2}\right) E_z = 0. \tag{5}$$

Inserting the expansion of Eq. 2 and 3 into Eq. 5 we obtain

$$(\mathbf{k} + \mathbf{G})^2 B(\mathbf{k}, \mathbf{G}) = \frac{\omega^2}{c^2}\tilde{\varepsilon}(0, \omega)B(\mathbf{k}, \mathbf{G}) + \frac{\omega^2}{c^2}\sum_{\mathbf{G} \neq \mathbf{G}'} \tilde{\varepsilon}(\mathbf{G} - \mathbf{G}', \omega)B(\mathbf{k}, \mathbf{G}'). \tag{6}$$

We are now in a position to insert the expansion coefficients $\tilde{\varepsilon}$ given by Eq. 4. We consider two geometries. The metallic core case is the configuration where the cores of the cylinders are metallic, i.e., permittivity given by Eq. 1, and are covered by shells of constant permittivity. The metallic shell case is the configuration in which the cores of the cylinders are modeled by a constant permittivity and the shells are metallic. Introducing $\xi = \omega/c$, we arrive at the following non-linear equation for the metallic core case.

$$(\xi^3 \mathbf{C} - \frac{i\gamma}{c}\xi^2 \mathbf{C} - \xi \mathbf{D} - \mathbf{E})\mathbf{B}(\mathbf{k}) = \mathbf{0}, \tag{7}$$

where

$$(\mathbf{C})_{\mathbf{GG}'} = (\varepsilon_b f_2 + \varepsilon_i f_i + f_1)\delta_{\mathbf{GG}'} \quad + \quad 2f_1(1 - \varepsilon_b)\frac{J_1(|\mathbf{G} - \mathbf{G}'|R)}{|\mathbf{G} - \mathbf{G}'|R} \tag{8}$$
$$+ \quad 2f_i(\varepsilon_i - \varepsilon_b)\frac{J_1[|\mathbf{G} - \mathbf{G}'|(R+d)]}{|\mathbf{G} - \mathbf{G}'|(R+d)};$$

$$(\mathbf{D})_{\mathbf{GG}'} = \left[(\mathbf{k} + \mathbf{G})^2 + f_1\frac{\omega_p^2}{c^2}\right]\delta_{\mathbf{GG}'} + 2f_1\frac{\omega_p^2}{c^2}\frac{J_1(|\mathbf{G} - \mathbf{G}'|R)}{|\mathbf{G} - \mathbf{G}'|R}; \tag{9}$$

$$(\mathbf{E})_{\mathbf{GG'}} = \frac{i\gamma}{c}(\mathbf{k} + \mathbf{G})^2 \delta_{\mathbf{GG'}}. \tag{10}$$

For the metallic shell case we obtain the same non-linear equations, but the matrix elements are given by

$$(\mathbf{C})_{\mathbf{GG'}} = (\varepsilon_a f_1 + \varepsilon_b f_2 + f_i)\delta_{\mathbf{GG'}} \quad + \quad 2f_1(\varepsilon_a - \varepsilon_b)\frac{J_1(|\mathbf{G} - \mathbf{G'}|R)}{|\mathbf{G} - \mathbf{G'}|R} \tag{11}$$
$$+ \quad 2f_i(1 - \varepsilon_b)\frac{J_1[|\mathbf{G} - \mathbf{G'}|(R+d)]}{|\mathbf{G} - \mathbf{G'}|(R+d)};$$

$$(\mathbf{D})_{\mathbf{GG'}} = \left[(\mathbf{k} + \mathbf{G})^2 + f_i\frac{\omega_p^2}{c^2}\right]\delta_{\mathbf{GG'}} + 2f_i\frac{\omega_p^2}{c^2}\frac{J_1(|\mathbf{G} - \mathbf{G'}|R)}{|\mathbf{G} - \mathbf{G'}|R}; \tag{12}$$

The matrix $\mathbf{E}$ is the same in both cases.

The non-linear equation is equivalent to the following set of linear equations.

$$\begin{pmatrix} 0 & \mathbb{I} & 0 \\ 0 & 0 & \mathbb{I} \\ \mathbf{C}^{-1}\mathbf{E} & \mathbf{C}^{-1}\mathbf{D} & \frac{-i\gamma}{c}\mathbb{I} \end{pmatrix} \begin{pmatrix} \mathbf{B} \\ \mathbf{a} \\ \mathbf{b} \end{pmatrix} = \xi \begin{pmatrix} \mathbf{B} \\ \mathbf{a} \\ \mathbf{b} \end{pmatrix}. \tag{13}$$

The first two equations resulting from the matrix-vector multiplication in Eq. 13 define $\mathbf{a} = \xi\mathbf{B}$ and $\mathbf{b} = \xi^2\mathbf{B}$. The third equation is equivalent to Eq. 7. Eq. 13 has been diagonalized for k-vectors in the fundamental eighth of the first Brillouin zone. The resulting band structures are presented and discussed in Sec. 3.

3. Results and discussion

Band structures were obtained by diagonalization of Eq. 13 for 599 k-values from across the Brillouin zone. Convergence studies showed that results obtained using 441 plane waves and 1681 waves agreed to four significant figures. Thus, the band structures presented here were acquired with 441 plane waves. In all spectra presented here we plot $\omega a/2\pi c$ with the normalization convention $\omega_p a/2\pi c = 1$. In other words, we define the plasma frequency as $\omega_p = 2\pi c/a$ to make the problem scale-invariant. With this definition we can let a take any value as long as R and d are shifted accordingly to achieve the same filling factors. In our simulations we set $a = 1$. However, is should be noted that one can use more physical parameters, such as the bulk plasma frequency of a given metal. If one then chooses the lattice constant $a = 2\pi c/\omega_p$ and the filling factors are kept constant the results will be the same. In all studies the damping parameter $\gamma = .01\omega_p$. The lifetime is defined as $1/\tau = -2\text{Im}(\omega)$.

Band structures and lifetimes for two-component photonic crystals composed of metallic cylinders in vacuum with filling factors of .01 and .1 are presented in Fig. 2 to illustrate the trends observed as metallic fraction is increased. The near-degeneracy of the first and second bands along the $M - X$ direction and between the second and third bands along the $X - \Gamma$ direction in the case of the .01 filling fraction is broken as the filling fraction is increased (compare Fig. 2(a) and 2(d)). For small filling factors, the imaginary parts of the eigenvalue band structure at the symmetry points display discontinuous behavior (see Fig. 2(c)). This is because the cross-section of the wires is small; only exactly along the lines of symmetry of the Brillouin zone do multiple reflections occur resulting in the formation of standing waves, which significantly enhance the lifetime of the states. A general trend for all structures considered here is the decrease of lifetime with increase of metallic filling factor. For all values of the filling factor the band with the shortest lifetime is the lowest band, but as the fill factor is
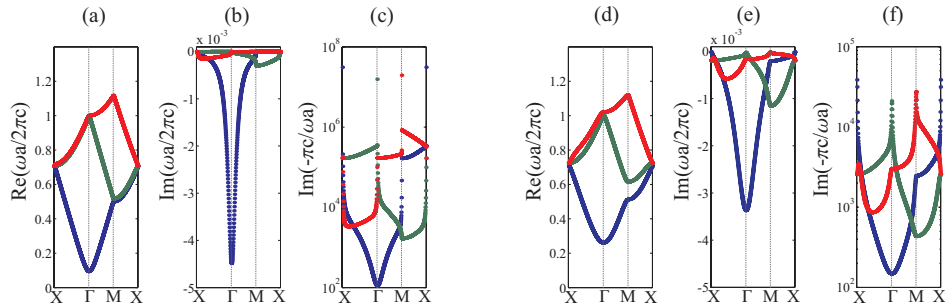
Fig. 2. The three lowest photonic bands of a two-component photonic crystal composed of metallic cylinders of filling factor .01 (a-c) and .1 (d-f) arranged in a square lattice. (a,d) The real part of the band structure. (b,e) The imaginary part of the band structure. (c,f) The lifetime of the states.

increased the lifetimes of higher bands become comparable to that of the lowest band. For the two-component photonic crystal with lossy metallic cylinders in vacuum all states—including the vacuum-like states above the plasma frequency—are damped meaning that the imaginary part of all eigenvalues is less than zero, corresponding to decay in time.

In Figs. 3-5 the real and imaginary parts of the band structures for two-component crystals, three-component metallic core and three-component metallic shell are juxtaposed for the cases where the filling factor of the metallic component is .1 and .6. It should be noted that in Figs. 3-5 six bands are plotted; however in Fig. 3 the y-axis extends to 1.6 whereas it is only necessary to extend it to 1.2 for the three-component cases. For sufficiently large filling factor the real part of the band structures of two-component photonic crystals composed of metallic cylinders in vacuum are characterized by two bandgaps, as seen in Fig. 3(b). From zero frequency to a cutoff there is a bandgap due to the inability of the E-polarized electromagnetic waves to propagate in the negatively permissive material. This bandgap is seen in Figs. 3-5. The size of this bandgap increases with the filling factor of the metallic component. The second bandgap occurs between the first and second bands. The bandgap between the first and second bands is clearly seen in Fig. 3(b). This bandgap is structural in that it is due to the production of standing waves caused by multiple reflections in the crystal; this bandgap can be observed in photonic crystals composed of dielectric cylinders, and the presence and size of this bandgap also depends on the filling factor. For photonic crystals composed of dielectric cylinders this bandgap will have a maximal value at a given filling factor generally different from the maximal filling factor. For the two-component plasmonic crystal the bandgap continues to increase as the fill factor is increased to its maximum value of .78. For fill factors above approximately .6 there is only one band below the plasma frequency, as is shown in Fig. 3(b). Above the plasma frequency, where the permittivity approaches unity, the dispersion relation shows the linear behavior one expects from electromagnetic waves propagating in vacuum.

In Fig. 4(b) one sees the structural bandgap has been filled, although the filling factor of the metal is still .6, as it was in Fig. 3(b). This closing of the structural bandgap between the second and third bands is characteristic of dielectric cylinders with increased filling factor and contrasts the behavior of purely metallic cylinders. In Fig. 5, where the metallic component is the outer shell of the cylinder, one sees an increase of the structural band gap, indicating the cylinder array maintains the character of metallic cylinders. However, in contrast to Fig. 3(b) there are four bands below the plasma frequency.

In Figs. 3-5 one can also see how the different structural configurations affect the group velocity of the propagating waves. For the lowest band in each case, the maximum of the group
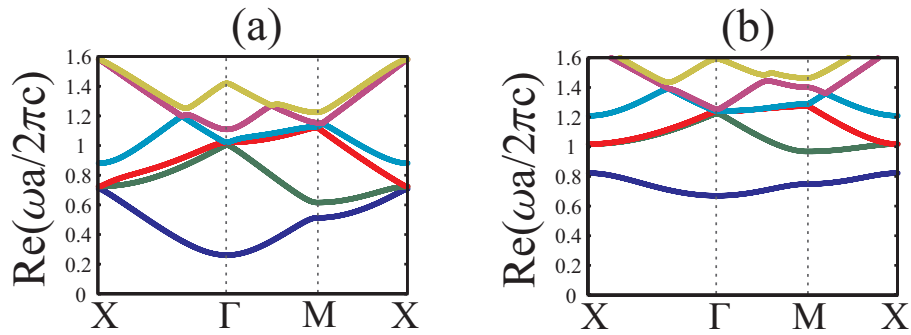
Fig. 3. The six lowest *E*-polarized photonic bands of a two-component photonic crystal composed of metallic cylinders arranged in a square lattice. (a) Metallic filling factor is .1. (b) Metallic filling factor is .6.
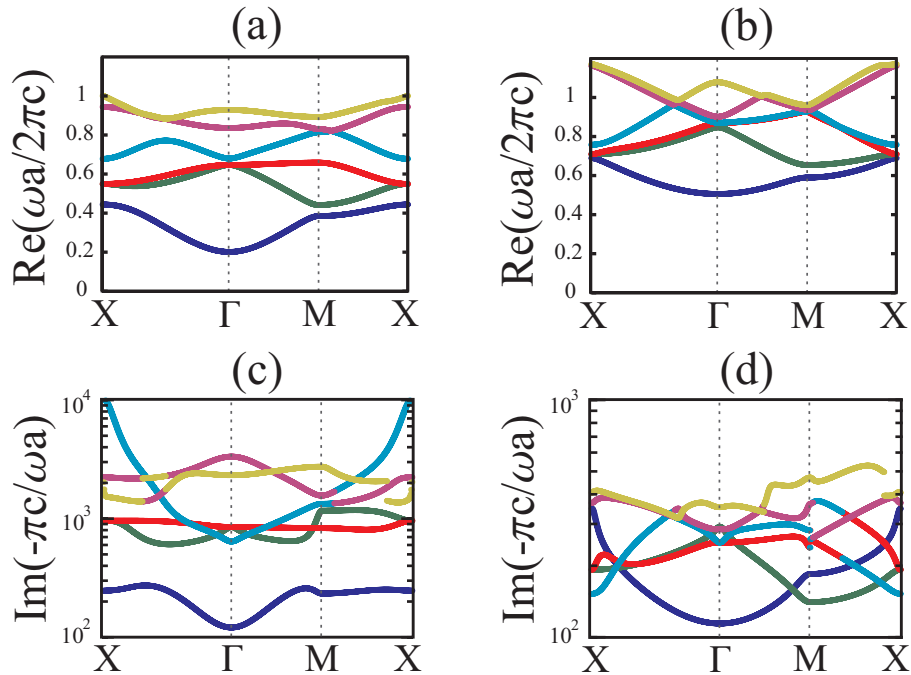

Fig. 4. The six lowest *E*-polarized photonic bands of a three-component photonic crystal composed of metallic cylinders surrounded by a dielectric shell of permittivity $\varepsilon = 12$ arranged in a square lattice. The filling factor of the dielectric is .1. (a,b) Real part of the band structure. (c,d) Lifetime of the states. (a,c) Metallic filling factor is .1. (b,d) Metallic filling factor is .6. Discontinuities in the imaginary parts of the band structure result from the fact that eigenvalues are sorted by real part of ω; when one lists the eigenvalues this way on either side of a band crossing and then plots a truncated number of bands, the imaginary parts of the eigenvalues can appear discontinuous.
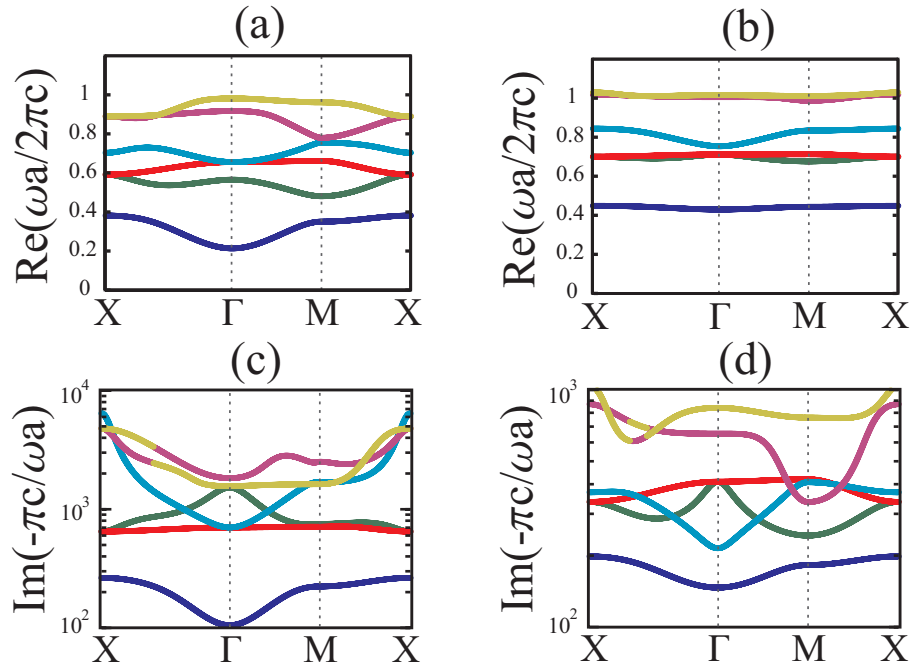
Fig. 5. The six lowest E-polarized photonic bands of a three-component photonic crystal composed of dielectric cylinders of permittivity $\varepsilon = 12$ surrounded by a metallic shell arranged in a square lattice. The filling factor of the dielectric is .1. (a,b) Real part of the band structure. (c,d) Lifetime of the states. (a,c) Metallic filling factor is .1. (b,d) Metallic filling factor is .6.

velocity occurs along the $X - \Gamma$ direction. For the two-component case with filling factor .6 (Fig. 3(b)) the maximum group velocity is $.3343c$, which is slightly less than $.4078c$, the value for the three-component metallic core case of the same metallic filling factor (Fig. 4(b)). However, the maximum group velocity of the lowest band for the three-component shell case (Fig. 5(b)) is $.0449c$, nearly an order of magnitude smaller. Such a trend continues up to and above the plasma frequency. The sixth band in both cases of three-component configurations is near the plasma frequency. In these two cases the maximum of the group velocity is along the $M - X$ direction. For the three-component metallic core case the maximum is $.5630c$ and for the metallic shell case the maximum is $.0672c$. These considerations indicate that of the three structural configurations considered in this study, the three-component metallic shell configuration is most effective in creating a medium where electromagnetic waves below the plasma frequency propagate with a significantly reduced group velocity. Above the plasma frequency all three cases demonstrate free-wave-like propagation as one would expect.

Inspection of the lifetimes of the propagating waves in the metallic core case versus the metallic shell case reveals the increase of metallic filling factor decreases the lifetimes for both geometries. Moving from Fig. 4(c) to 4(d) one observes that the lowest propagating band maintains a similar lifetime near the Γ point of the Brillouin zone and experiences an increase in lifetime with increased metallic filling factor near the X point due to the increase in group velocity with the closing of the structural band gap. However, all higher bands suffer a decrease in lifetime, some by as more than an order of magnitude. Moving from 5(c) to 5(d) one finds a similar lifetime near the Γ point and a reduced lifetime near the X point for the metallic shell
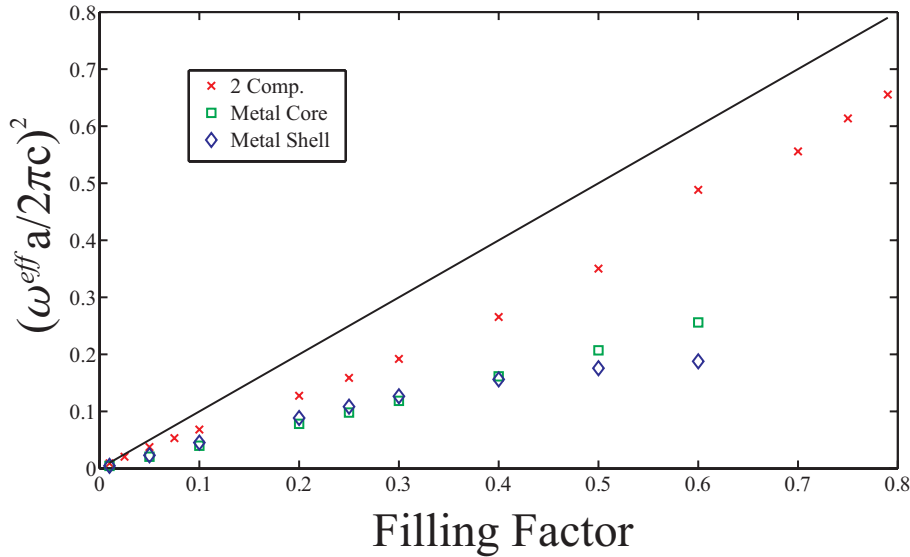
Fig. 6. The lowest propagating frequency of E-polarized modes for two-component, three-component metallic core and three-component metallic shell photonic crystals plotted as a function of filling factor of the metallic component of the cylinders. The filling factor of the dielectric components is .1.

case. Still, the lifetime of the lowest band across the Brillouin zone is not affected dramatically by increasing the metallic filling factor from .1 to .6, but the lifetimes of higher bands are more significantly affected.

For all cases considered here the lowest allowed frequency for a propagating mode increases with increasing filling factor of the metallic component. It is interesting to compare the values of this cutoff frequency as a function of filling factor for the three cases considered here. As a basis for comparison, we note that $\omega_p = \sqrt{Ne^2/m\varepsilon_0}$ where N is the electron density, e is the electron charge and m is the electron mass. We can define an effective plasma frequency for the crystal given by $\omega_p^{eff} = \sqrt{N_{eff}e^2/m\varepsilon_0}$ where $N_{eff} = fN$. Here f is the filling factor of the metallic component of the crystal. Thus, $(\omega_p^{eff})^2 = f\omega_p^2$, or, invoking the normalization we have been using $(\omega_p^{eff}a/2\pi c)^2 = f$. Therefore, if the lowest allowed frequency of a propagating mode were determined by this effective plasma frequency we should see a linear relationship between the square of the normalized cutoff frequency and the filling factor. In Fig. 6 we show the lowest allowed propagating frequency plotted against the filling factor for the two and three-component photonic crystals. In all cases, the lowest allowed frequency falls below the line $(\omega_p^{eff}a/2\pi c)^2 = f$ and in both the cases of the metallic core and the metallic shell the lowest allowed frequency for a given filling factor falls below that for the two-component case.

It is interesting to consider which aspects of the data presented in Figs. 2-6 can be explained by consideration of light propagating in an effective index environment, which can be explained by consideration of the resonant properties of individual cylinders and which must take into account the complete structural configuration including the core/shell structure of the cylinders and the geometric arrangement of the cylinders into a lattice. For wavelengths much longer than the lattice constant of the array the electromagnetic waves experience an average material medium; inability of light to propagate below the lowest band—a phenomenon which occurs in the metallic shell and core structures as well as in the two-component cylinders—can be under-

stood in the effective index picture. In the metallic core case, the structural band gap closes with increased filling factor. This is a feature of dielectric photonic crystals. Thus, one may be inclined to assume the features of the structural band gap are governed by the exterior layer of the cylinders. Another feature, the significant flattening of the bands with increased filling factor, only occurs in the metallic shell case. While it seems apparent that the crystalline arrangement gives rise to the structural band gap, which arises in two-component photonic crystals as well, the slow group velocity seems to be unique to the shell structures. In order to gain more insight into the relation between the slow group velocity and the resonances of individual cylinders one would need to have an understanding of the resonances of the individual metallic shell cylinders. Individual metallic cylinders coated with dielectric have scattering cross sections with may features [20]. Because metallic shell cylinders have two exposed surfaces, surface plasmons may be excited on both surfaces and may hybridize to give rise to even more complicated scattering cross sections [21]. Understanding how the resonances of the constituent cylinders contribute to the slow group velocity of the array is a worthwhile pursuit but is beyond the scope of this work.

4. Closing remarks

We have considered light propagation in two-dimensional arrays of metallodielectric cylinders. Unique features of band structures were analyzed. In particular, covering the metallic cylinders in a dielectric shell was shown to close the structural bandgap as the filling factor of the metal core was increased. However, the presence of a dielectric core in a metal cylinder did not have the same effect on the band structure. Photonic crystals composed of metallic shells surrounding dielectric cores were shown to significantly flatten the photonic bands below the plasma frequency indicating the creation of a medium in which light propagates with an anomalously slow group velocity. Bands with a maximum group velocity of $.05c$ were discovered. In the same structure, the maximum group velocity of any band below the plasma frequency was approximately $.06c$, with the exception of one band which had a group velocity of $.3c$ near the Γ point of the Brillouin zone.

In closing it is important to note that analysis of this system requires consideration of a large parameter space. This study is by no means meant to be an exhaustive account of the possibilities of the system, rather as an illustration of the significance of the arrangement of the components of a three component plasmonic crystal, not just the filling factors.

A. Numerical considerations

All common methods for calculating band structures become more cumbersome when dispersion is introduced. The non-linearity in the eigenproblem resulting from the introduction of the eigenvalue, ω, into the derivation necessitates diagonalization of a $3N \times 3N$ matrix within the formalism utilized in this study. This decreases the computational efficiency of the plane wave method for calculating band structures of dispersive systems.

For all cases of E-polarization considered in this study, satisfactory convergence was achieved. Up to 1681 plane waves were used, and the difference in the real parts of the eigenvalues calculated using 441 and 1681 plane waves was approximately $.005\%$ for the lowest bands and $.05\%$ for bands near ω_p. Convergence of the imaginary parts was equally satisfactory.

Although the tripling of the matrix slows the calculations, several aspects of the problem can speed the calculation. The calculation time is linear in k; because the diagonalization for a given k is independent of diagonalization for all other k', the calculation is easily parallelizable. Also, for the case of circular cylinders with infinite extent in one spatial dimension arranged in a square lattice, the $N \times N$ sub-matrices comprising the larger $3N \times 3N$ matrix are highly symmetric. This can be seen from an analysis of the reciprocal lattice vectors which serve as
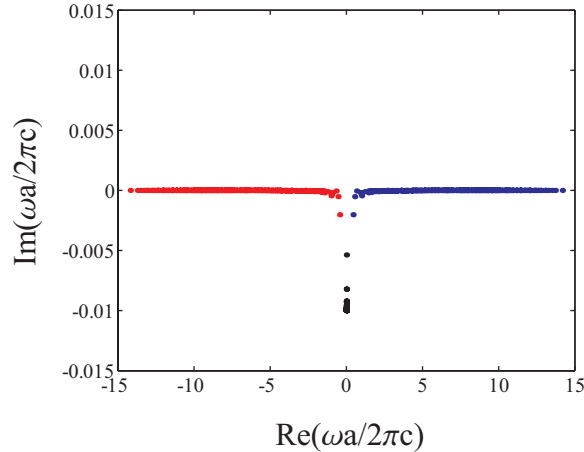
Fig. 7. The eigenvalue spectrum for *E*-polarization plotted in the complex plane for a metallic core surrounded by a dielectric shell with $\varepsilon_i = 12$. The filling factor of each component is .1. The first *N* eigenvalues are plotted in red and have $\mathrm{Re}(\omega) < 0$. The second *N* are in black and have $\mathrm{Re}(\omega) \approx 0$. The third *N* are in blue with $\mathrm{Re}(\omega) > 0$.

indices to the matrix elements $\mathbf{G} = m\mathbf{b}_1 + n\mathbf{b}_2$ where $\mathbf{b}_i$ is a primitive vector of the reciprocal lattice. If *m* and *n* each take $\tilde{N}$ different values, then $N = \tilde{N}^2$. The $N \times N$ sub-matrices (Eqns. 8-12) are indexed by $\mathbf{G}$ and $\mathbf{G}'$. For the square lattice, the reciprocal lattice is simply a Cartesian mesh. The $N \times N$ sub-matrices are each themselves comprised of $\tilde{N} \times \tilde{N}$ sub-matrices, each of which is a Toeplitz matrix. These sub-sub-matrices are themselves arranged in a Toeplitz matrix to fill the sub-matrix. Thus, calculation of each sub-matrix only requires calculation of the first row of the matrix and utilization of the Toeplitz symmetry. Since the matrix elements require calculation of Bessel functions, it is a great advantage to calculate only *N* matrix elements rather than N^2. Incorporating this symmetry into the calculation speeds it up significantly so that virtually all of the time required to carry out the calculation is during diagonalization. Calculating the matrix elements and filling the matrices is nearly instantaneous.

In Figs. 7, 8 and 9 we plot several eigenvalue spectra at the *X* point of the Brillouin zone in the complex plane. Figure 7 shows all 3*N* eigenvalues of Eq. 9 for the case of a metallic core of filling factor .1 covered by a dielectric shell of filling factor .1 and $\varepsilon_i = 12$. The first *N* of these states have negative real part and negative imaginary part approaching zero as the real part becomes more negative. The second *N* have very small real part and negative imaginary part. The third *N* have the same imaginary parts as the first *N* but positive real parts. It is the third *N* which have been plotted as the physical spectrum throughout this paper. The spectrum appears to have symmetry with respect to change of sign of the real part of the eigenvalues. In fact, in the absence of a dielectric shell or core the second *N* eigenvalues are noise at the level of 10^{-15} and if treated as zero the spectrum does have symmetry with respect to change of sign of the real part. When a dielectric component is accounted for in the eigenproblem the second *N* eigenvalues develop a band structure at the 10^{-9} level, and this very low frequency band structure is convergent with increasing basis size.

Figure 8 shows a spectrum for the same configuration as Fig. 7, but with a dielectric core of $\varepsilon_1 = 12 - .1i$. Here we see a breaking of symmetry between positive and negative values of real part—in fact the first and third *N* eigenvalues of the spectrum develop an antisymmetry. The third *N* states develop significant positive values of imaginary part of eigenfrequency while the third *N* acquire significant negative imaginary parts. Figure 9 displays the spectrum for the same
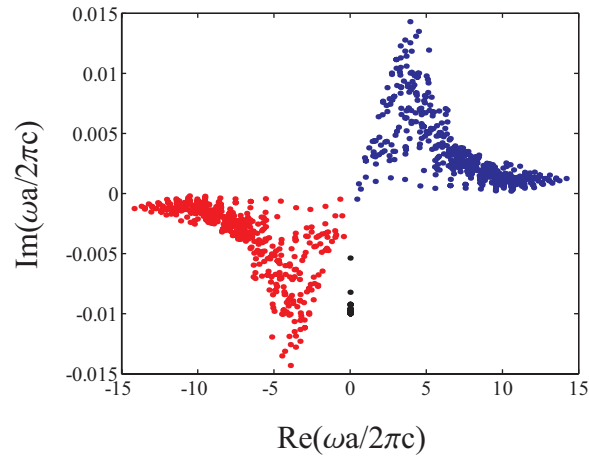
Fig. 8. The eigenvalue spectrum for *E*-polarization plotted in the complex plane for a metallic core surrounded by a dielectric shell with $\varepsilon_i = 12 - .1i$. The filling factor of each component is .1. The first N eigenvalues are plotted in red and have $\mathrm{Re}(\omega) < 0$. The second N are in black and have $\mathrm{Re}(\omega) \approx 0$. The third N are in blue with $\mathrm{Re}(\omega) > 0$.
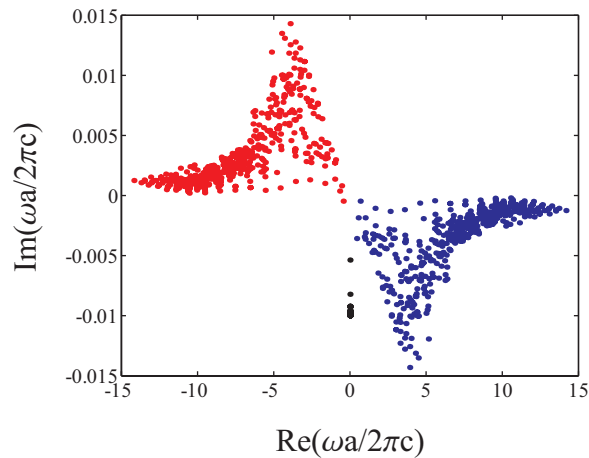

Fig. 9. The eigenvalue spectrum for *E*-polarization plotted in the complex plane for a metallic core surrounded by a dielectric shell with $\varepsilon_i = 12 + .1i$. The filling factor of each component is .1. The first N eigenvalues are plotted in red and have $\mathrm{Re}(\omega) < 0$. The second N are in black and have $\mathrm{Re}(\omega) \approx 0$. The third N are in blue with $\mathrm{Re}(\omega) > 0$.

case as the previous two figures but with $\varepsilon_i = 12 + .1i$. The spectrum is antisymmetric, as in Fig. 8, but with the first N now having positive imaginary parts. In all three figures the tendency for large values of $\mathrm{Re}(\omega)$ to be associated with small values of $\mathrm{Im}(\omega)$ is demonstrated. This results from the decreased damping of the metal with increasing $\mathrm{Re}(\omega)$. The imaginary part of the permittivity of the metallic component is given by

$$\mathrm{Im}[\varepsilon(\omega)] = \frac{\gamma \omega_p^2}{\omega^3 + \gamma^2 \omega},\tag{14}$$

and so metallic damping decays as ω^{-3}.

B. Acknowledgments